Computational Analysis of the Flow and Acoustic Effects of Jet-Pylon Interaction

Craig A. Hunter[*], Russell H. Thomas[†], K.S. Abdol-Hamid[◊], and S. Paul Pao[✣]
NASA Langley Research Center, Hampton VA, 23681 USA

Alaa A. Elmiligui [‡]
Analytical Services and Materials, Hampton VA, 23666 USA

Steven J. Massey [§]
Eagle Aeronautics, Hampton VA, 23669 USA

Computational simulation and prediction tools were used to understand the jet-pylon interaction effect in a set of bypass-ratio five core/fan nozzles. Results suggest that the pylon acts as a large scale mixing vane that perturbs the jet flow and jump starts the jet mixing process. The enhanced mixing and associated secondary flows from the pylon result in a net increase of noise in the first 10 diameters of the jet's development, but there is a sustained reduction in noise from that point downstream. This is likely the reason the pylon nozzle is quieter overall than the baseline round nozzle in this case. The present work suggests that focused pylon design could lead to advanced pylon shapes and nozzle configurations that take advantage of propulsion-airframe integration to provide additional noise reduction capabilities.

Nomenclature

Symbols

BPR	=	bypass-ratio
D	=	core nozzle diameter (m)
$d\bar{A}$	=	area vector differential element (m^2)
k	=	turbulent kinetic energy (TKE) per unit mass (m^2/s^2)
M	=	Mach number
NPR	=	nozzle pressure ratio
P_o	=	stagnation pressure (N/m^2)
ϕ	=	normalized total temperature
φ	=	mass-averaged normalized total temperature
ρ	=	density (kg/m^3)
T_o	=	stagnation temperature (°K)
$\bar{u}$	=	velocity vector (m/s)
U	=	streamwise (axial) velocity component (m/s)
X	=	streamwise coordinate (m)
Y	=	vertical coordinate (m)
Z	=	spanwise coordinate (m)

Subscripts

core	=	core flow
fan	=	fan flow
∞	=	freestream

---

[*]   Aerospace Engineer, Configuration Aerodynamics Branch, MS 499
[†]   Senior Research Engineer, Aeroacoustics Branch, MS 166, Senior Member AIAA
[◊]   Aerospace Engineer, Configuration Aerodynamics Branch, MS 499, Associate Fellow AIAA
[✣]   Senior Research Engineer, Configuration Aerodynamics Branch, MS 499, Associate Fellow AIAA
[‡]   Senior Scientist, 107 Research Drive, AIAA Member
[§]   Senior Research Scientist, 13 West Mercury Blvd, AIAA Member

I. Introduction

Over the past several decades there has been a continued focused effort to reduce engine component source noise in order to reduce the highest levels of noise of commercial subsonic transport aircraft. More recently, as engine sources were reduced in large part by high bypass ratio (BPR) engines, sources of airframe noise have also been investigated because of their importance at approach conditions. In addition to these engine and airframe sources, other means of reducing the total aircraft system noise impact on the community have been brought to the forefront of research as additional increments of noise reduction are increasingly difficult to attain.

One opportunity for additional increments of noise reduction centers on the aeroacoustic effects of propulsion airframe integration, that is, propulsion airframe aeroacoustics (PAA). PAA has been relatively underdeveloped and represents an area of potential noise reduction technologies for conventional configurations. This opportunity includes both reducing the noise sources that arise specifically from integration of propulsion and airframe, and also using the installation itself as a means to reduce noise of a particular airframe or propulsion source[1].

In general, the propulsion airframe aeroacoustic effects that can be identified are many and can be grouped in various ways. Fundamentally, effects can be grouped into those issues having to do with flow interaction and those having to do with acoustic propagation, although these are not entirely unrelated issues. Flow interaction effects are caused by the flow field of one component interacting with another specifically because of the location or orientation of installation. An example of this is the influence of the engine mounting pylon on the core jet exhaust flow. These types of flow interaction effects from installation can create new acoustic sources or they can modify existing acoustic sources already associated with the components.

Jet noise from a conventional engine-under-wing configuration typically has installation effects, due to both flow interactions and acoustic propagation, from the pylon, wing, and flap interaction, along with jet noise reduction devices. Chevron nozzles are an example of a jet noise reduction device that has been studied extensively for isolated jets in recent years[2]. The influence of the pylon on a jet creates flow features that are not present in an isolated jet. One area of research, therefore, has been toward understanding effects of the jet-pylon interaction including the effects on chevron noise reduction devices.

There have been several experimental efforts recently in the area of jet-pylon interaction. Bhat[3] studied the azimuthal effects of a pylon by testing a 1/20th scale model of a bypass ratio five separate flow nozzle to measure the effect of the pylon and bifurcator relative to the baseline axisymmetric nozzle. The effect of adding the bifurcator was found to add 0.5 EPNdB (static, data flown at M=0.24) to 1.0 EPNdB (at M=0.24) relative to the baseline. With the pylon installed, an azimuthal directivity of about 2 EPNdB was measured at low power settings and 3.5 EPNdB was measured at high power settings. No chevron nozzles were included in this study.

Martens[4] included a chevron core nozzle and a pylon in the test of a bypass ratio five separate flow nozzle. The chevron core nozzle produced about a 2-3 EPNdB reduction compared to the baseline core nozzle for this 1/11th scale model of the CFM56–5B exhaust system. Differences of 1-2 EPNdB were noticed for both baseline and chevron nozzles, at the two azimuthal angles tested corresponding to sideline and cutback conditions.

An additional study by Thomas and Kinzie[5] measured the effect of a pylon on bypass ratio five and eight nozzles including chevron nozzles. For the bypass ratio five configuration, the addition of the pylon reduced the noise by approximately 1 EPNdB compared to the baseline case and there was little effect of azimuthal angle, not significantly above the level of repeatability. The core chevron produced a 1.8 EPNdB reduction compared to the baseline nozzle. Adding a pylon to the chevron core nozzle produced a reduction in the benefit of the core chevrons. For the bypass ratio eight configuration, adding a pylon to the baseline nozzle increased the noise at higher cycle points, but adding a pylon to the core chevron nozzle had little effect.

The experimental results of Thomas and Kinzie have been used in rigorous validations of computational fluid dynamics (CFD) simulation of the mean flow field using PAB3D[6,7] and the installed jet noise prediction capability of Jet3D[8]. These flow field simulations and noise predictions have provided a valuable database of detailed information. The previous work showed the quantitative ability of these tools to predict the approximately 1 EPNdB noise reduction due to the BPR 5 jet-pylon interaction, and the present study will use the existing validated flow

field and noise prediction database to provide an understanding of the flow and acoustic effects attributable to the jet-pylon interaction. In the current work, PAB3D and Jet3D will be used as exploration and visualization tools rather than their typical role as predictive data generation tools. The reader is encouraged to consult previous reports[6-8] for the detailed information that the present study is based on.

II.   Background

A. Nozzle Configurations
The separate flow BPR 5 nozzle configurations used in this study are shown in Figures 1 and 2, and consist of a baseline round core and fan nozzle (configuration 1) and a round core and fan nozzle with a pylon and lower fan bifurcator strut (configuration 6). Each 1/9th scale nozzle has a nominal core exit diameter of D=0.128m. The nozzle and pylon designs are not from a specific engine, but rather, they are typical of BPR 5 engines (additional details of the nozzle configurations can be found in References 5-7). In past and present work, the nozzles were operated at a takeoff condition with the following nominal settings:

$$Core\ Nozzle:\ NPR=1.56,\ T_{o,core}=828°K$$

$$Fan\ Nozzle:\ NPR=1.75,\ T_{o,fan}=359°K$$

$$Freestream:\ P_{o,\infty}=101353N/m^2,\ T_{o,\infty}=295°K,\ M_{\infty}=0.28$$

B. Computational Fluid Dynamics Simulation
The Reynolds-Averaged Navier-Stokes (RANS) CFD simulations of Massey, et al.[6] were used to generate mean flow information and serve as input data for noise prediction with Jet3D. These simulations were run with the PAB3D multi–block structured flow solver[9], using temperature-corrected two-equation k-ε turbulence closure[10] and a linear Reynolds stress model. Grid sizes ranged from 5.8 million cells for the half-span grid of configuration 1 up to 11.4 million cells for the half-span grid of configuration 6. In both cases, the computational domain extended roughly 32D downstream of the fan nozzle exit and 6D from the centerline in the radial direction. As discussed by Massey, et al.[6], CFD predictions were in excellent agreement with experimental mean flow total temperature and total pressure data.

C. Jet Noise Prediction
The Jet3D software[8,11] was used for noise prediction and jet noise source diagnostics. Jet3D is based on a modern implementation of Lighthill's Acoustic Analogy (LAA) with anisotropic Reynolds stress modeling, and has been developed to handle complex three-dimensional turbulent flows and installed jet configurations. As discussed by Hunter and Thomas[8], Jet3D SPL predictions were in good agreement with experimental noise measurements in the inlet arc for configurations 1 and 6. Jet arc predictions were good up to about 121° inlet angle, beyond which Jet3D under predicted low frequency SPL levels (due to inherent limitations in the implementation of LAA used in Jet3D). Jet3D predicted full-scale-equivalent EPNL for configurations 1 and 6 to within the standard deviation band of measured data. Furthermore, Jet3D captured the effect of the pylon, correctly predicting a reduction in EPNL of approximately 1 EPNdB.

III.   Results and Discussion

A. Flow Effects
Contours of normalized total temperature are plotted for configurations 1 and 6; figures 3 and 4 show the total temperature in the streamwise symmetry plane, while figures 5 and 6 show total temperature in cross-stream planes located at X/D=2, 5, 8, and 12. Examination of these plots shows a very basic characteristic of the jet-pylon interaction in configuration 6 – the pylon induces the core stream upward. The resulting core flow takes on a cardioid-like shape at X/D=5 and 8, but reverts back towards a circular shape at X/D=12.

Analogous plots of turbulent kinetic energy (TKE) per unit volume are given in figures 7-10. Here, the presence of turbulence indicates mixing between the various streams. Note that, in both configurations, turbulence is concentrated in the fan-freestream shear layer (indicating mixing between the two streams) and there is very little

turbulence in the core-fan shear layer (indicating little mixing between these two streams). In both configurations, the core and fan streams merge around X/D=6 to 7, and the jet is fully developed (turbulence reaching centerline) by X/D=11 or so. In terms of TKE per unit volume, the jet-pylon effect manifests itself in a modified shear layer shape (i.e., compare figures 9 and 10) and regions of intensified turbulence downstream of the pylon.

More details of the jet-pylon interaction are shown in figures 11 and 12, where cross-flow streamlines are drawn over a contour plot of axial velocity (U) at X/D=8 for configurations 1 and 6, respectively. Streamlines in figure 11 are typical for a developed co-axial jet resulting from an annular core/fan nozzle, and show inward entrainment flow from the freestream, outward flow from the fan stream, and inward flow from the core stream (classical features of a co-axial jet flow). Rings formed where the streamlines collapse represent midpoints of shear layers where flow is moving entirely in the axial direction. The lower half of the configuration 6 jet in figure 12 shows these same characteristics, but the upper half of the jet is dramatically different because of the jet-pylon interaction. In this region, the jet flow is characterized by two pairs of counter-rotating streamwise vortices with associated secondary flow, and streamlines from the freestream are seen to penetrate deep down into the center of the jet. In both cases, the magnitude of cross-flow velocities was on the order of 0-3% of the axial velocity, making secondary flows rather weak. In the case of configuration 6, however, the weak secondary flows are enough to disrupt the formation of a traditional cross-flow shear layer streamline pattern in the top half of the jet. The lower vortex pair shown in figure 12 corresponds to the regions of intensified turbulence shown in figure 10 at X/D=8.

Additional streamline patterns for configuration 6 are shown in figure 13; here, oil flow lines are shown on the nozzle and pylon, and volume streamlines are shown on the centerline symmetry plane. In this figure, it is very easy to see upward turning flow along the pylon side, and upward flow on the symmetry plane downstream of the pylon. This view also shows that the upper core flow in the symmetry plane is clearly attached to the pylon underside "shelf", and the annular core stream is lopsided in favor of the pylon. All of these signs support the existence of a coanda-like effect between the core flow and the curved pylon shelf. As core flow exits past the pylon, the upwards trajectory, combined with a fan flow that has been parted by the pylon, results in a "rooster-tail" type of upwash and gives rise to the crossflow streamline patterns seen in figure 12. The jet-pylon interaction effect is shown schematically in figure 14, and suggests that the pylon is acting like a mixing vane, creating large scale asymmetry and secondary flows in the jet.

The large scale vortices shown in figure 12 can be traced to the jet-pylon interaction, but the vortices do not originate directly from the geometry in a traditional sense (among other things, the rotational direction of the vortices is not consistent with vortex rollup or the formation of horseshoe vortices, and pylon oil flow lines show no sign of separation). The lower vortex pair is formed between X/D=2 and X/D=3, as shown in figures 15 and 16. Here, the vortical flow is actually an "eddy" in the two-dimensional crossflow view, formed as downward entrainment flow from outside the jet turns upward due to the pylon upwash effect. The upwash enters into the jet flow behind the pylon where the pylon shelf ends at X/D=2.5. A similar mechanism results in the upper vortex pair forming behind the pylon tip at X/D=4.3. So, the vortical flows do not originate directly from the pylon geometry itself through a separation, rollup, or shedding mechanism. Rather, they are formed by the pylon upwash field in combination with the jet entrainment flow, when unobstructed by the pylon. This understanding provides the explanation of one of the experimental results obtained in the acoustic tests of these configurations[5]. A large fillet was added to configuration 6 at the junction of the pylon and core body with the intent of mitigating an expected horseshoe vortex, but the results reported[5] showed no noise impact of the fillet.

Crossflow streamlines are shown at X/D=20 for configurations 1 and 6 in figures 17 and 18, respectively. Once again, streamlines for the round nozzle (configuration 1) are typical of a developed and mixed jet, with inward entrainment flow from the freestream and outward flow from the jet centerline. In this case, at X/D=20, there is only one shear layer ring visible as the core and fan streams have mixed and merged prior to this point. Streamlines for configuration 6 in figure 18 show a similar flow pattern, but the shear layer forms a pear-shaped ring that is narrower and elongated on the bottom as compared to the round nozzle's circular shear layer ring (an estimate of the shear layer perimeter showed it to be roughly the same in both cases). Though there is significantly less secondary flow in the configuration 6 jet at X/D=20 when compared to earlier stations (figures 12, 15, 16), there is still a fair amount of swirling flow compared to the round jet of configuration 1.

An overall measure of jet mixing is given in figure 19, where the mass-averaged non-dimensional total temperature parameter of Kenzakowski et al.[12] is plotted versus X/D. The parameter is computed as follows:

$$\varphi = \frac{\int \phi \rho \bar{u} \cdot d\bar{A}}{\int \rho \bar{u} \cdot d\bar{A}} \tag{1}$$

where

$$\phi = \frac{T_o - T_{o,fan}}{T_{o,core} - T_{o,fan}} \tag{2}$$

The integration is carried out for $0.005 \leq \phi \leq 1.000$, which covers the jet from the core stream (ϕ=1.000) to the edge of the fan stream (ϕ=0.005). The resulting parameter gives the decay of the core temperature as the core and fan streams mix. As shown in figure 19, the pylon jet from configuration 6 begins to out-mix the round jet from configuration 1 at approximately X/D=2.5, the location where the pylon ends and the secondary flows (discussed above) begin. Another interesting feature to note is the knee in the curve for configuration 1 at X/D=5.5 to 6; this coincides with the merging of the nozzle shear layers discussed above in conjunction with figures 7 and 9. By X/D=13, the round jet mixing catches up with the pylon jet when both jets become fully developed. In the context of the overall temperature decay, the pylon can be said to "jump start" the mixing process, but this effect only exists for about the first 10 diameters past the end of the pylon.

B. Acoustic Effects
Contours of mean-square acoustic pressure per unit volume over all frequency bands in a 1/3 octave scale ranging from 80Hz to 100kHz are shown in figures 20-23. To generate these plots, OASPL mean-square acoustic pressure contributions computed for an observer on a 100D radius at an inlet angle of 88° along the jet sideline were traced back to source locations in the jet, normalized by the source volume, and plotted to show a map of noise sources in the jet. Figures 20 and 21 show noise source maps in the centerline symmetry plane for configurations 1 and 6, respectively, while figures 22 and 23 show similar maps in planes at X/D=8 and 12.

Comparing figures 20 and 21 shows an interesting result of the jet-pylon interaction – noise, which was evenly balanced between upper and lower shear layers in configuration 1, decreases in the lower shear layer and intensifies in the upper shear layer in configuration 6. This is consistent with the upward motion of the jet flow in the wake of the pylon. Noise sources are seen to be concentrated behind the pylon.

Noise maps in figures 22 and 23 show additional acoustic effects of the jet pylon interaction. In both plots, there is a basic side-to-side noise asymmetry due to spatial phasing in Lighthill's acoustic analogy[8], which distinguishes between near and far sides of the jet relative to the observer (located at Z/D=100 in the plots). Noise sources for the round configuration in figure 22 show only this basic asymmetry, while features of the jet-pylon interaction are evident beyond the basic asymmetry in figure 23. Figure 24 gives a closer look at the relative noise differences between the two configurations by subtracting the noise source map of configuration 1 from the noise source map of configuration 6. At X/D=8, the jet-pylon interaction upwash and secondary flows in configuration 6 are seen to manifest themselves in significant noise increases in the upper half of the jet and significant noise decreases in the lower half of the jet. At X/D=12, there are small regions of weakly increased noise near the centerline and at the outer regions of the jet, but the majority of the jet shows a substantial noise decrease.

To supplement these local snapshots of noise, an OASPL histogram is shown in figure 25, where noise from every 0.25D "slice" of the jet is shown from X/D=0 to X/D=30. Essentially, this figure sorts OASPL noise contributions from the jet based on their X/D location, in bins of one-quarter jet diameter. Here, the OASPL levels of configuration 6 have been adjusted to account for the reduction in flow area due to the pylon in order to make an even comparison between the two configurations. The resulting plot shows that the pylon jet (configuration 6) starts out quieter, but noise levels jump up at approximately X/D=3, right after the pylon ends at X/D=2.5. From about X/D=3.5 to X/D=10, the pylon jet makes more noise than the round jet, but from X/D=10 all the way downstream, the pylon jet is quieter than the round jet by about 0.5 dB per 0.25D slice of the jet. This sustained reduction in noise is likely what makes the pylon jet quieter overall[8].

There are several other features in the noise histogram worth discussing. First, there seems to be a linkage between the knee in the mass averaged total temperature curve (figure 19) at X/D=6 for configuration 1 and the sudden increase in noise for the same configuration at X/D=7 in figure 25. As discussed previously, the knee forms as the fan and core shear layers begin merging at X/D=6, and this appears to foreshadow a resulting increase in noise one diameter further downstream at X/D=7. This is similar to the end of the pylon at X/D=2.5 foreshadowing an increase in noise at X/D=3 (discussed above), and suggests a general 0.5D to 1D lag between flow/geometry changes and a subsequent effect on noise (this lag is likely due to turbulence development). Finally, both configuration 1 and configuration 6 have well defined noise peaks in the histogram; the former at X/D=10.5 and the latter at X/D=9.5. These peaks correlate well with noise source maps shown in figures 20 and 21.

All of these observations further the notion that the pylon jump starts the mixing process within the first 10D of the jet's development. This generates more noise upstream along with an earlier noise peak, but results in less noise downstream and less noise overall. Thus, the pylon acts as a noise reduction device in this case. Since the current nozzles are based on a generic design with no specific noise reduction goals, this work suggests that additional focused PAA design work can lead to advanced pylon shapes and configurations that result in even deeper noise reduction capabilities by taking advantage of the jet-pylon interaction.

IV.   Conclusion

In this study, computational simulation and prediction tools were used to understand the jet-pylon interaction effect in a set of BPR 5 core/fan nozzles. Results suggest that the curved pylon shelf creates a coanda-effect that draws core flow upward and creates a rooster-tail upwash in the wake of the pylon. This mechanism sets up vortical secondary flows in the jet and jump starts the jet mixing process in the first 10 diameters of the jet's development. In a sense, the pylon acts as a large scale mixing vane that perturbs the jet flow.

Noise source diagnostics were used to look at the detailed acoustic effect of the jet-pylon interaction. While the enhanced mixing and associated secondary flows from the pylon result in a net increase of noise upstream in the jet, there is a sustained reduction in noise extending from X/D=10 all the way downstream. This is likely the reason the pylon nozzle is quieter overall than the baseline round nozzle in this case.

Since previous studies have shown positive and negative acoustic effects associated with jet-pylon interaction, this is clearly a nozzle- and configuration-dependent effect. The present work focuses on a situation where the jet-pylon interaction can be beneficial for noise reduction. In this particular case, nozzles were based on a generic design with no specific noise reduction features. Focused pylon design work could lead to advanced pylon shapes and nozzle configurations that provide additional noise reduction capabilities and take advantage of propulsion-airframe integration for even deeper noise reduction. Though the current work focused only on flow and acoustic effects, performance should be a key factor in any future pylon design work for noise reduction.

Acknowledgement

References

[1]Thomas, R. H. "Aeroacoustics of Propulsion Airframe Integration: Overview of NASA's Research." Noise-Con Paper 105, presented at the 2003 Noise-Con, Cleveland, Ohio, June 23-25, 2003.

[2]Saiyed, N., Mikkelsen, K., and Bridges, J., "Acoustics and Thrust of Separate-Flow Exhaust Nozzles with Mixing Devices for High Bypass Ratio Engines." AIAA Paper 2000-1961.

[3]Bhat, T.R.S. "Experimental Study of Acoustic Characteristics of Jets from Dual Flow Nozzles." AIAA Paper 2001-2183.

[4]Martens, S. 2002 "Jet Noise Reduction Technology Development at GE Aircraft Engines." ICAS Paper 842, presented at the International Council of the Aeronautical Sciences, September, 2002.

[5]Thomas, R.H. and Kinzie, K.W. "Jet-Pylon Interaction of High Bypass Ratio Separate Flow Nozzle Configurations." AIAA Paper No. 2004-2827.

[6]Massey, S.J., Thomas, R.H., Abdol-Hamid, K.S., and Elmiligui, A. "Computational and Experimental Flowfield Analyses of Separate Flow Chevron Nozzles and Pylon Interaction". AIAA-2003-3212, May 2003.

[7]Thomas, R.H., Kinzie, K.W., and Pao, S.P. "Computational Analysis of a Pylon-Chevron Core Nozzle Interaction." AIAA-2001-2185, May 2001.

[8]Hunter, C., and Thomas, R. "Development of a Jet Noise Prediction Method for Installed Jet Configurations." AIAA Paper No. 2003-3169.

[9]Pao, S.P., and Abdol-Hamid, K.S. "Numerical Simulation of Jet Aerodynamics Using a Three Dimensional Navier Stokes Method (PAB3D)". NASA TP-3596, September 1996.

[10]Abdol-Hamid, K., Pao, S., Massey, S., and Elmiligui, A. "Temperature Corrected Turbulence Model for High Temperature Jet Flow." ASME Journal of Fluids Engineering, Vol. 126, No 5, September 2004.

[11]Hunter, C. "An Approximate Jet Noise Prediction Method Based on Reynolds-Averaged Navier-Stokes Computational Fluid Dynamics Simulation." D.Sc. Dissertation, The George Washington University, January, 2002.

[12]Kenzakowski, D.C., Shipman, J., Dash, S. M., Bridges, J.E., and Saiyed, N.H. "Turbulence Model Study of Laboratory Jets with Mixing Enhancements for Noise Reduction." AIAA Paper 2000-0219, 2000.

American Institute of Aeronautics and Astronautics
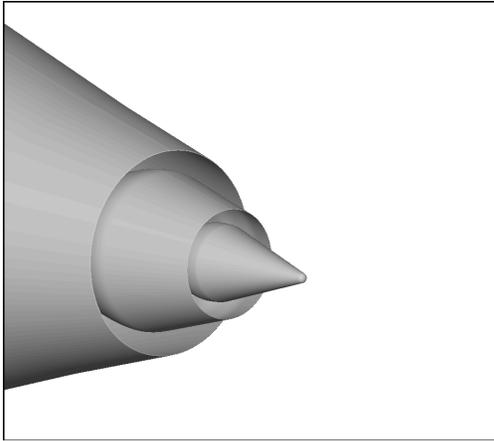
Figure 1: Configuration 1 Nozzle
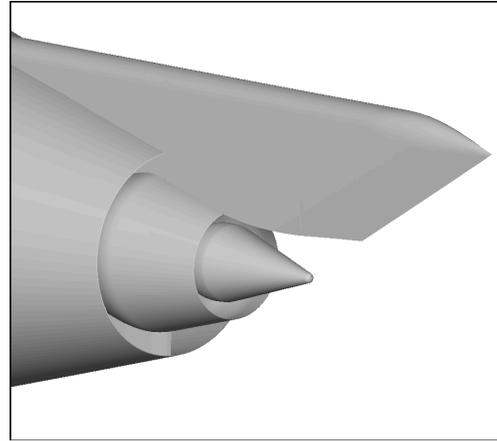
Figure 2: Configuration 6 Nozzle
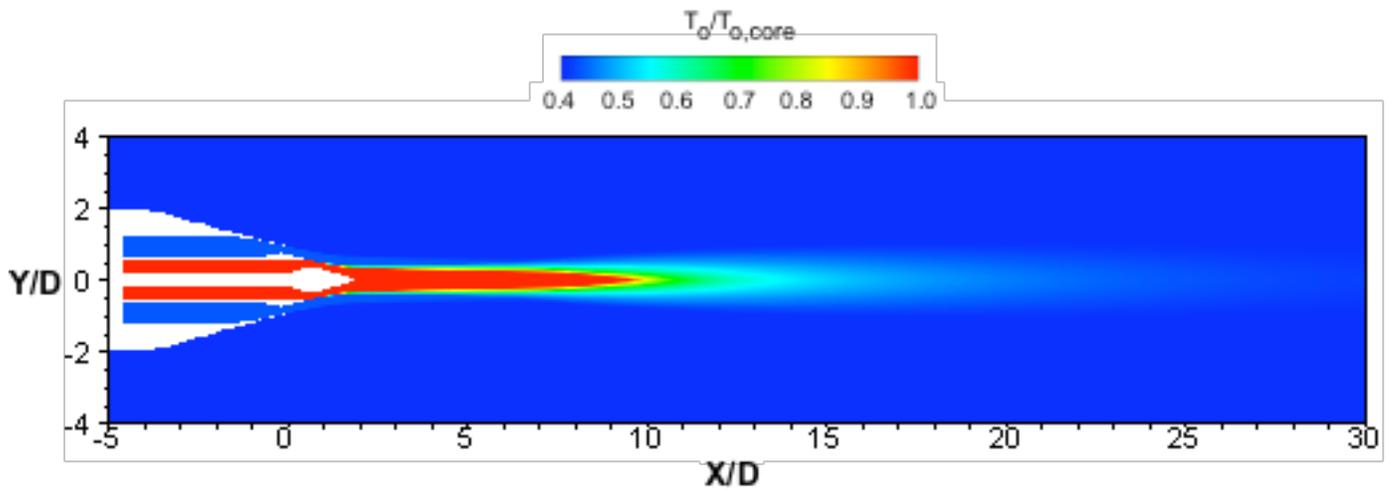


Figure 3: Normalized total temperature, configuration 1
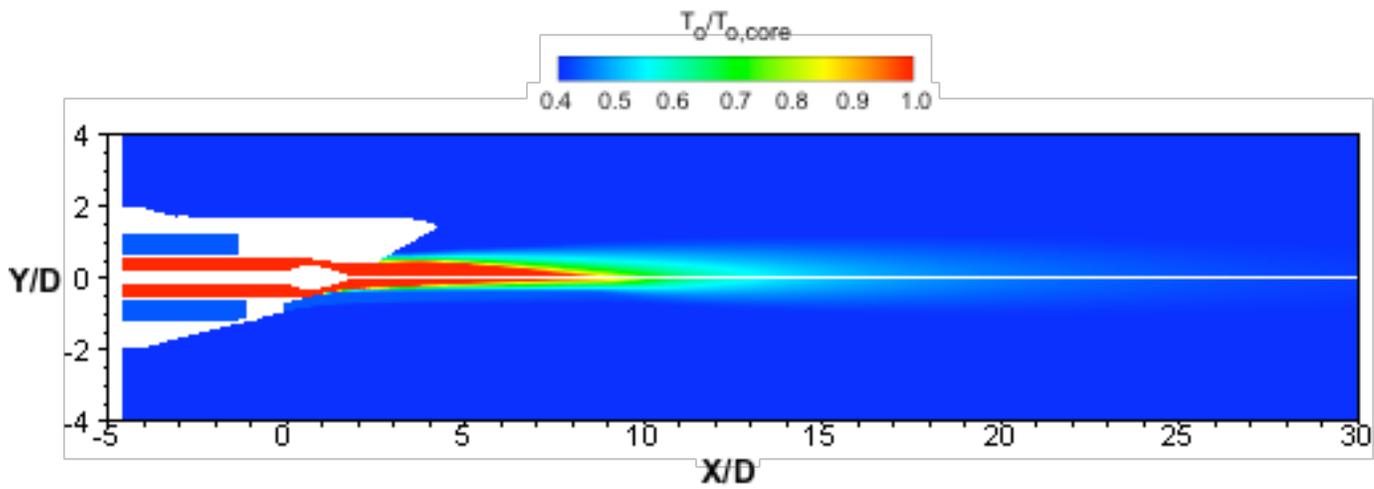
**Figure 4: Normalized total temperature, configuration 6**

American Institute of Aeronautics and Astronautics
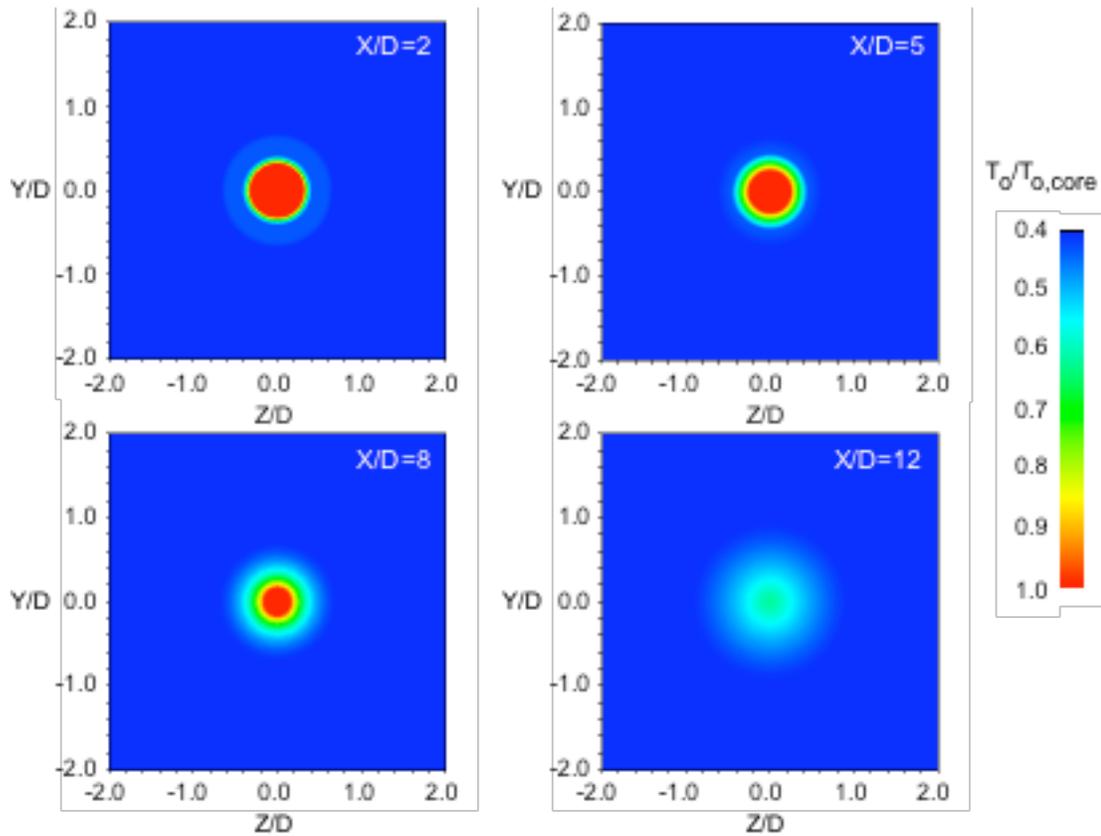
Figure 5: Normalized total temperature, configuration 1
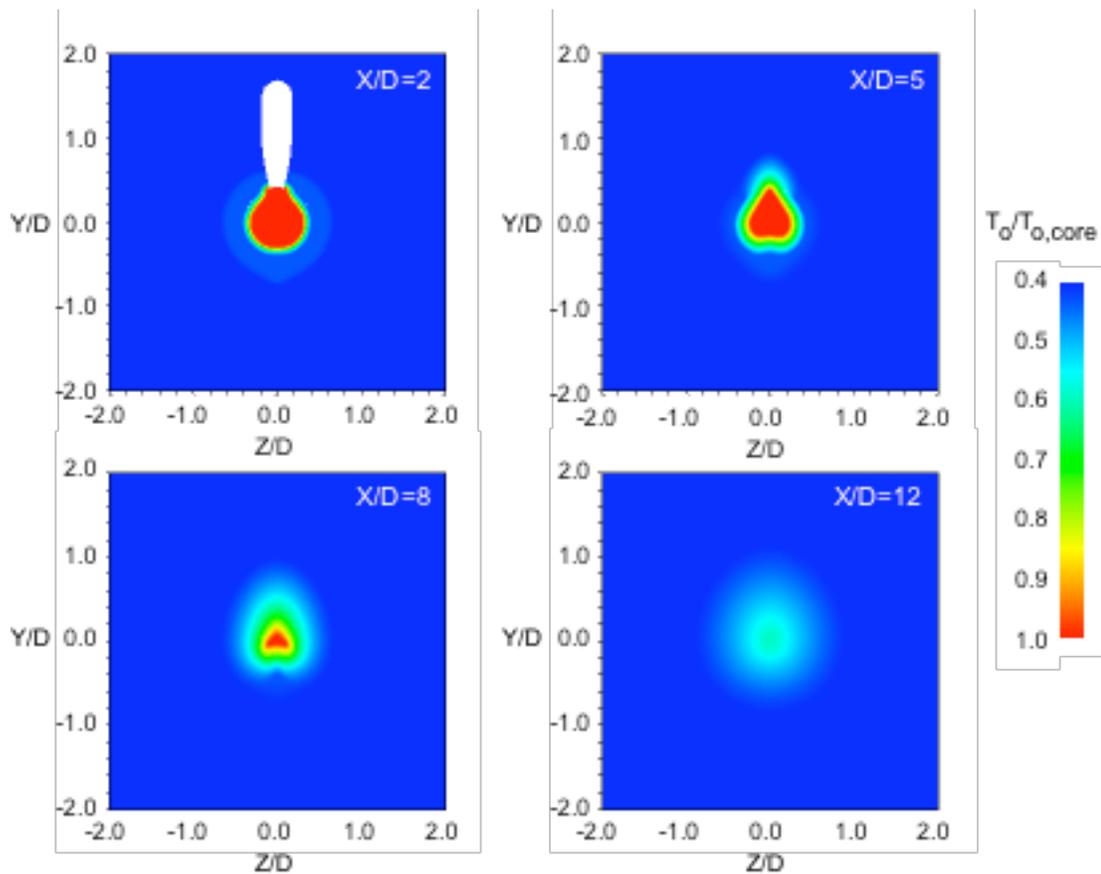
Figure 6: Normalized total temperature, configuration 6

American Institute of Aeronautics and Astronautics
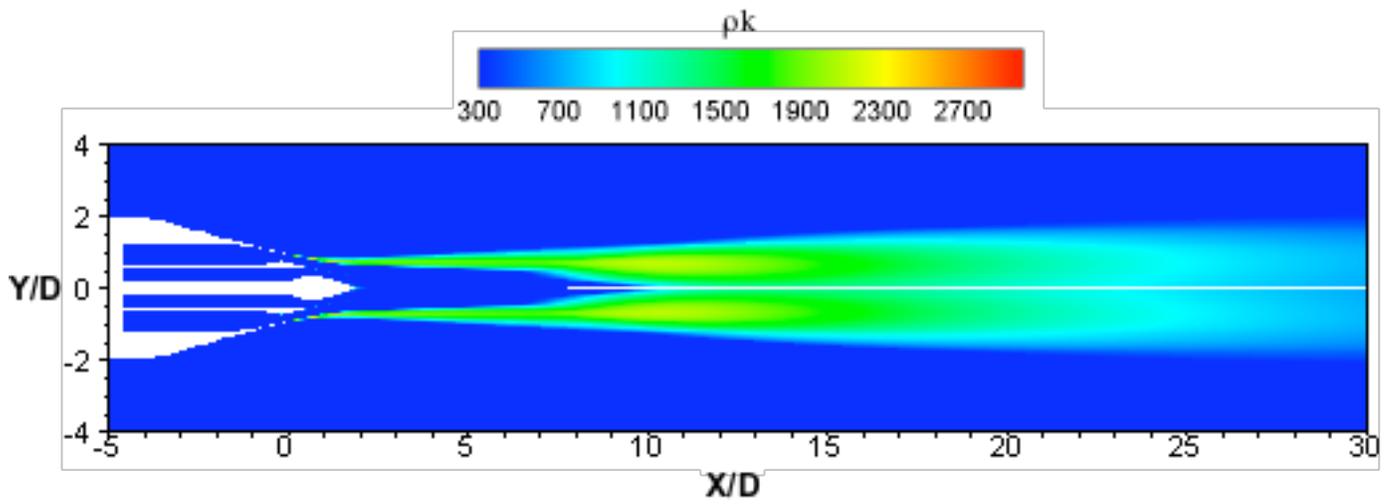
Figure 7: Turbulent kinetic energy per unit volume (kg/ms^2), configuration 1
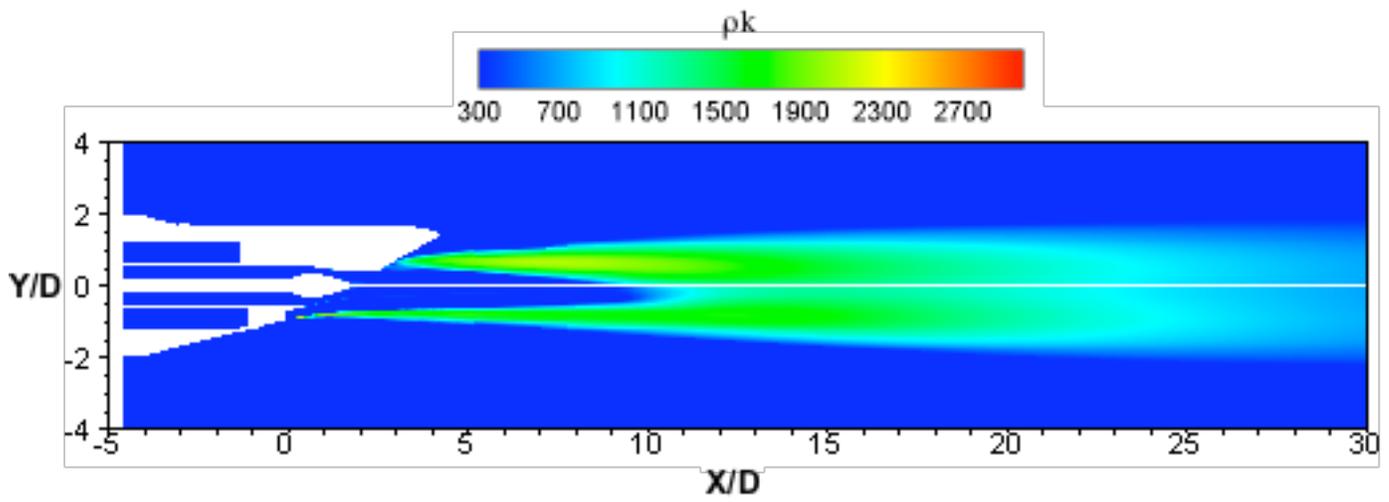
Figure 8: Turbulent kinetic energy per unit volume (kg/ms^2), configuration 6
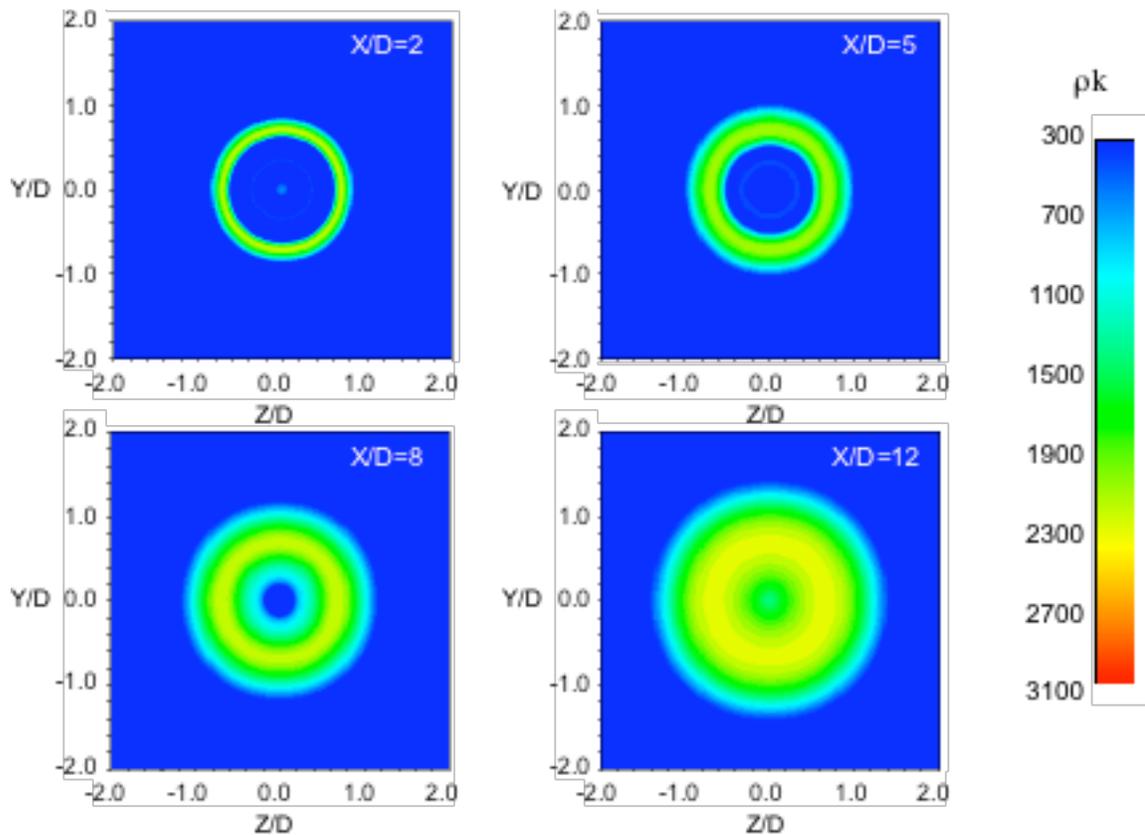
Figure 9: Turbulent kinetic energy per unit volume (kg/ms²), configuration 1
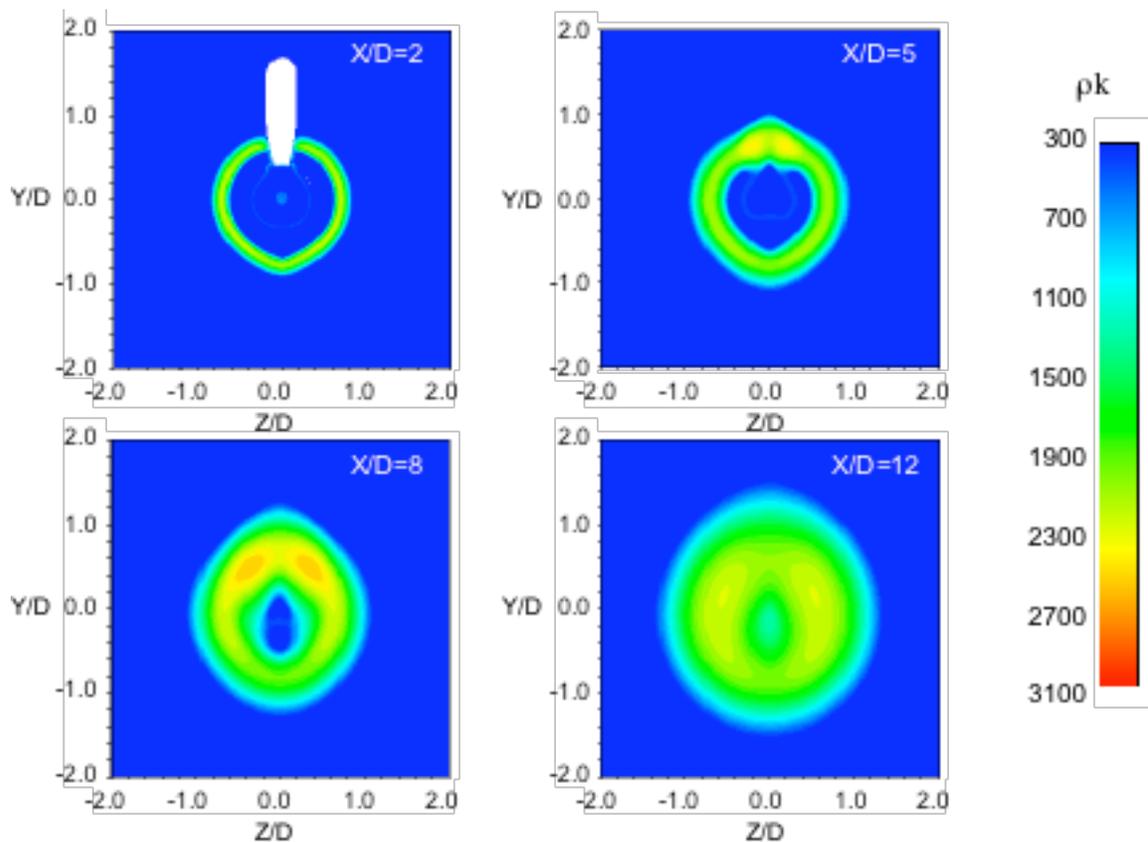
Figure 10: Turbulent kinetic energy per unit volume (kg/ms²), configuration 6

American Institute of Aeronautics and Astronautics
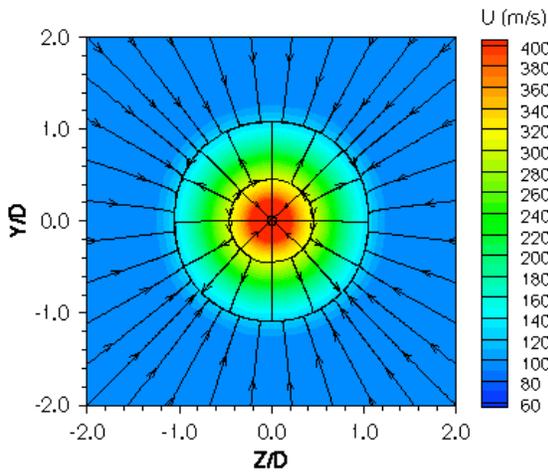
Figure 11: Crossflow streamlines for configuration 1 at X/D=8
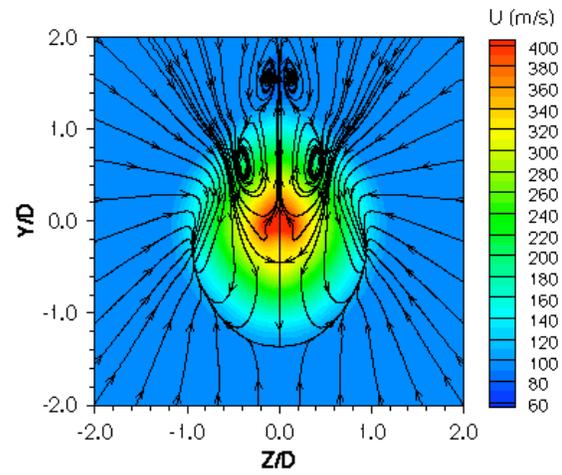
Figure 12: Crossflow streamlines for configuration 6 at X/D=8
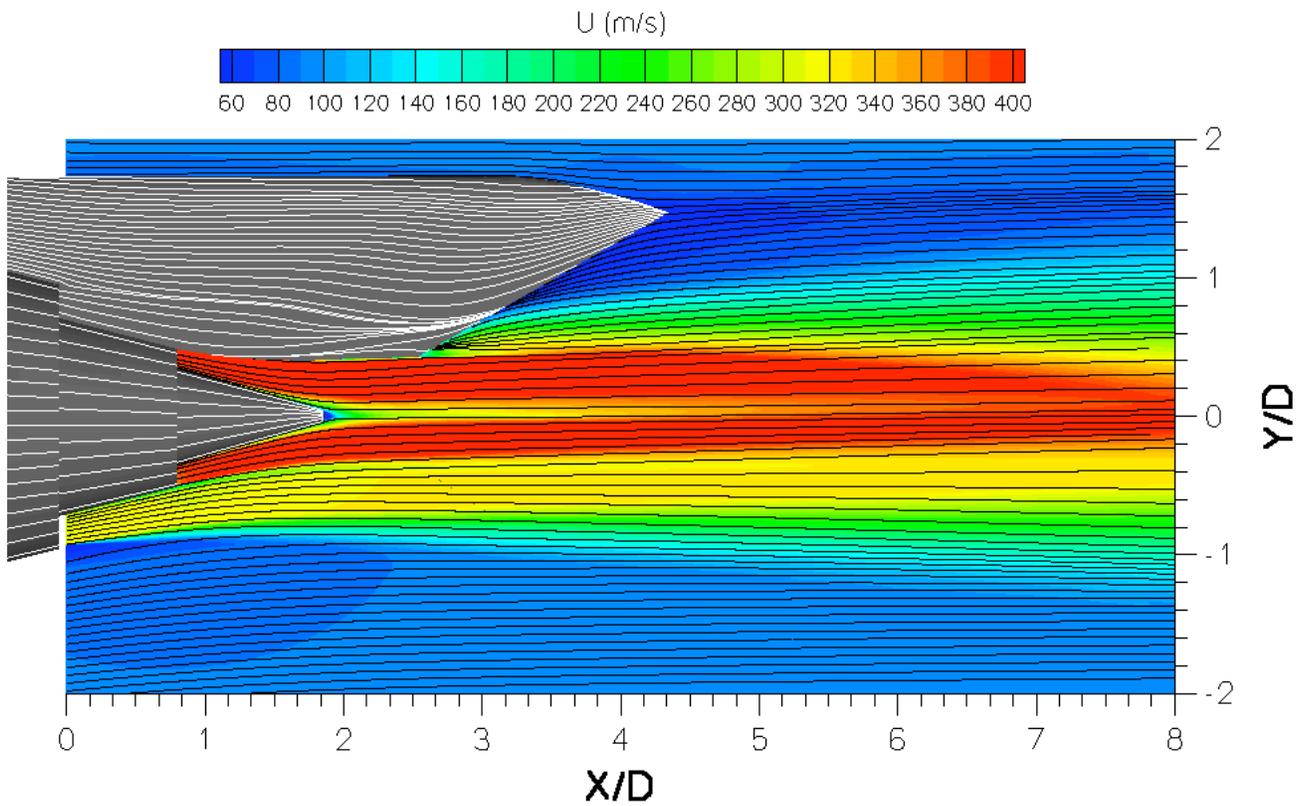
Figure 13: Streamlines on nozzle surface and symmetry plane, configuration 6. Note: all streamlines are pointing in the general downstream direction.
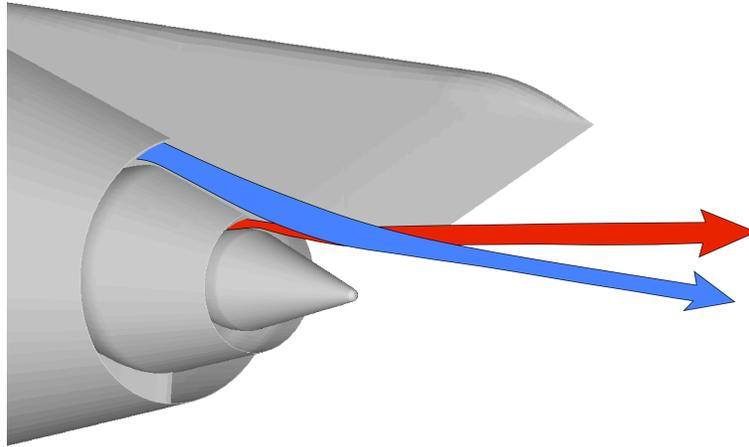
Figure 14: Schematic of the jet-pylon interaction "rooster-tail" effect
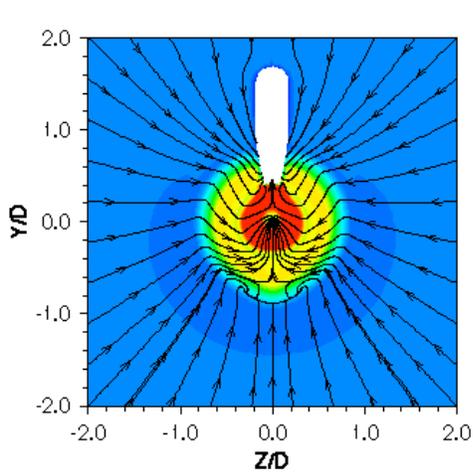
Figure 15: Crossflow streamlines for configuration 6 at X/D=2
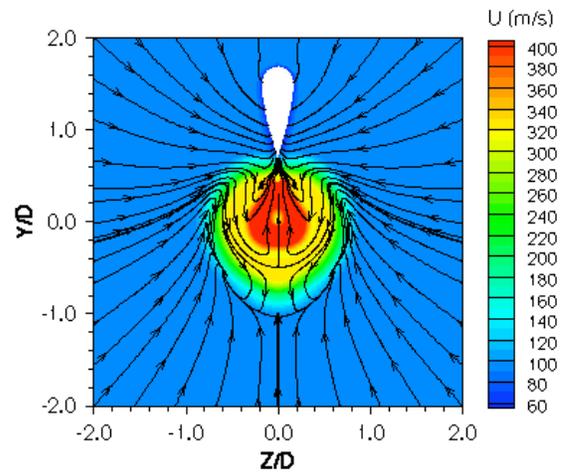
Figure 16: Crossflow streamlines for configuration 6 at X/D=3
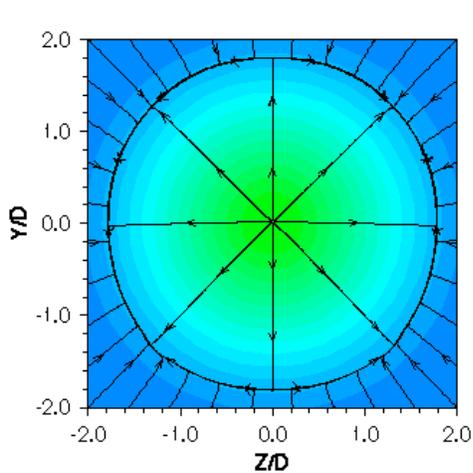
Figure 17: Crossflow streamlines for configuration 1 at X/D=20
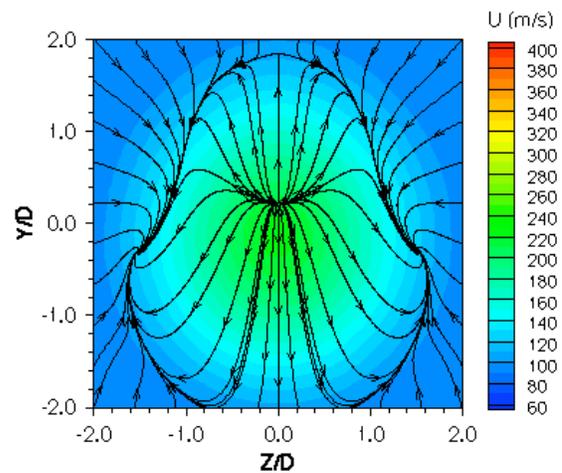
**Figure 18: Crossflow streamlines for configuration 6 at X/D=20**

American Institute of Aeronautics and Astronautics
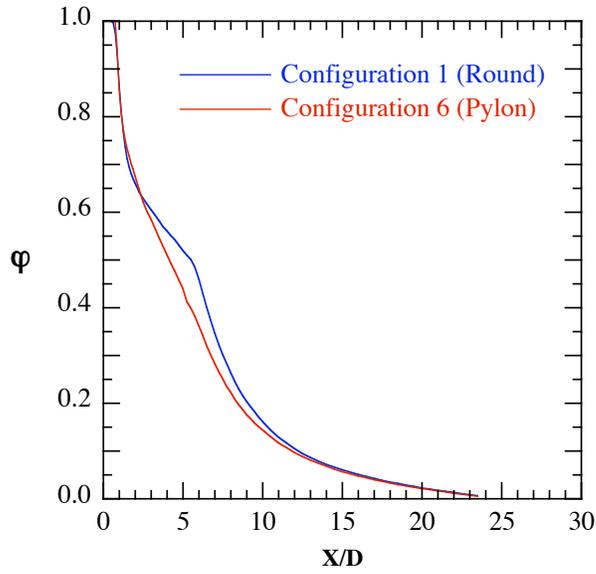
Figure 19: Mass-averaged non-dimensional total temperature for configurations 1 and 6
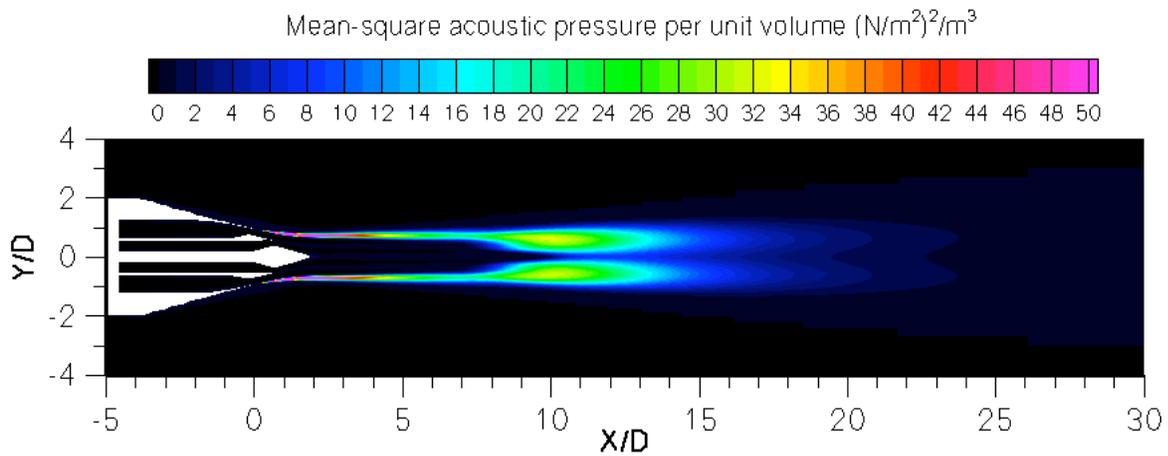
**Figure 20: Symmetry plane noise source map for configuration 1**
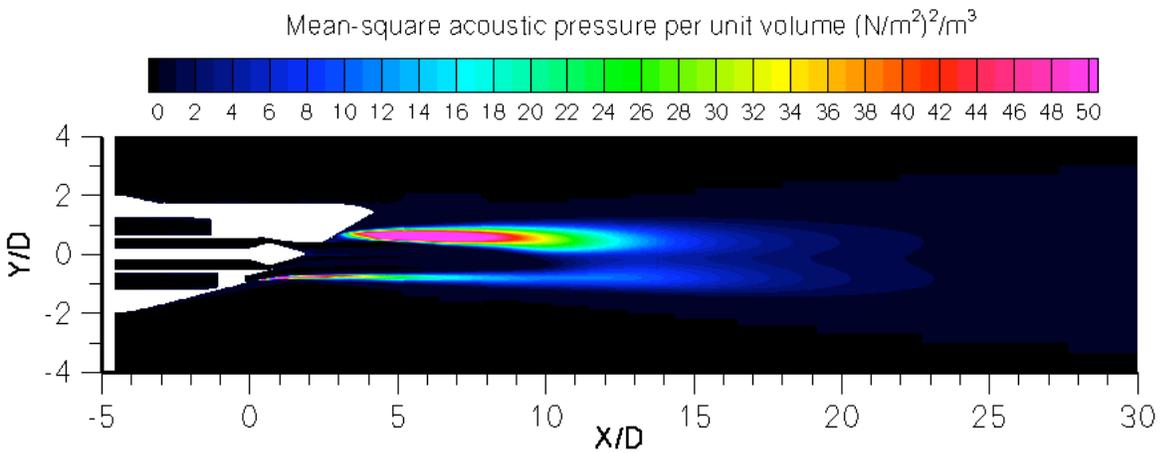
**Figure 21: Symmetry plane noise source map for configuration 6**

American Institute of Aeronautics and Astronautics

Mean-square acoustic pressure per unit volume $(N/m^2)^2/m^3$

0 2 4 6 8 10 12 14 16 18 20 22 24 26 28 30 32 34 36 38 40 42 44 46 48 50
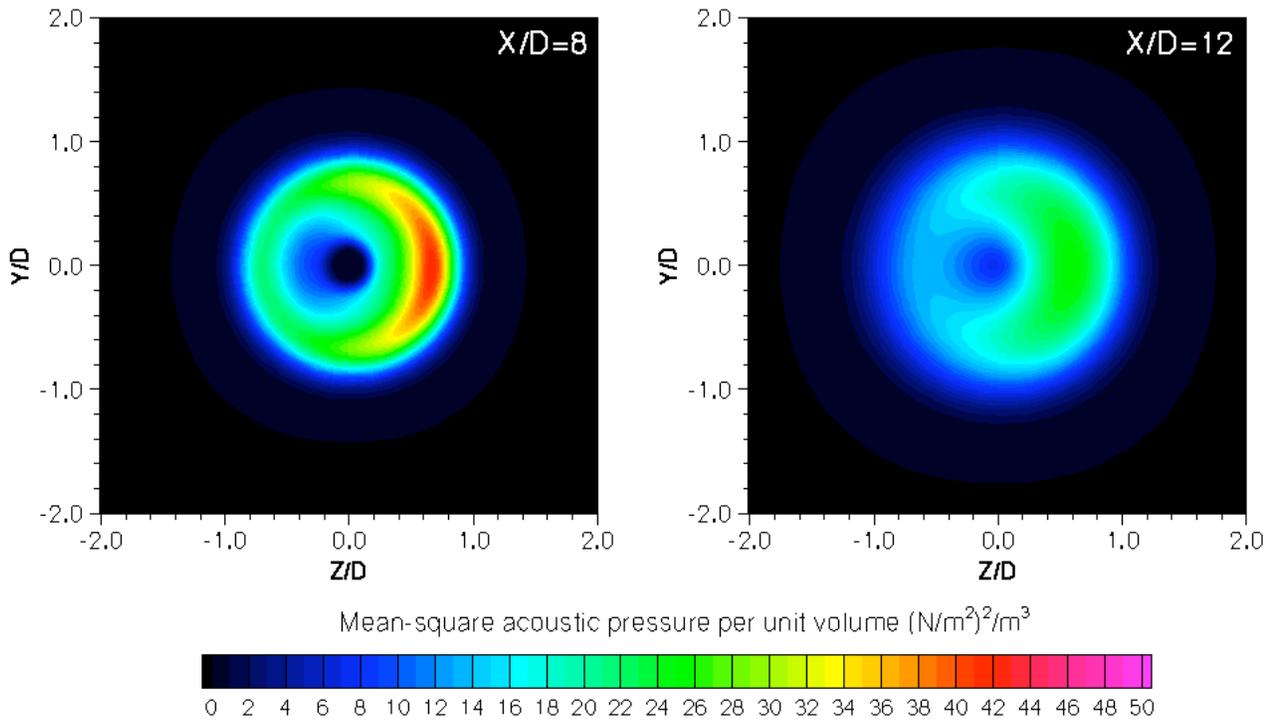
Figure 22: Noise source map for configuration 1 at X/D=8 and 12

Mean-square acoustic pressure per unit volume $(N/m^2)^2/m^3$

0 2 4 6 8 10 12 14 16 18 20 22 24 26 28 30 32 34 36 38 40 42 44 46 48 50
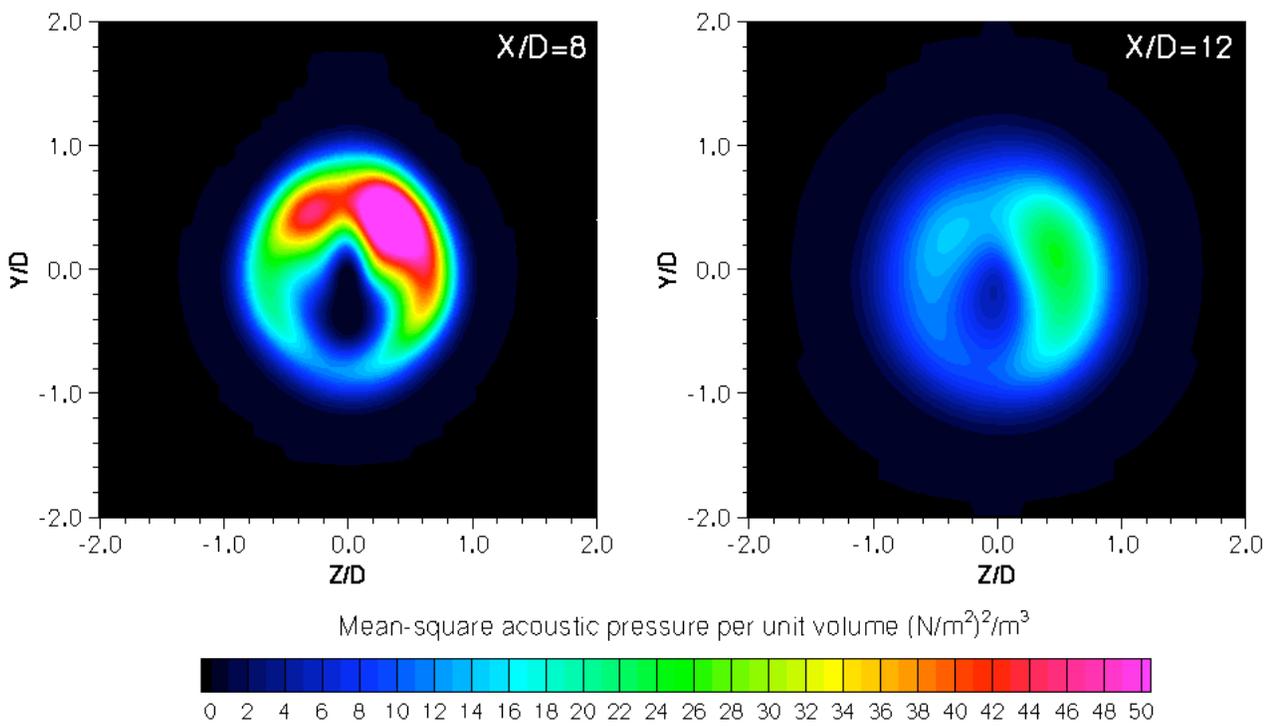
Figure 23: Noise source map for configuration 6 at X/D=8 and 12

Mean-square acoustic pressure difference per unit volume (N/m²)²/m³
(Configuration 6 - Configuration 1)
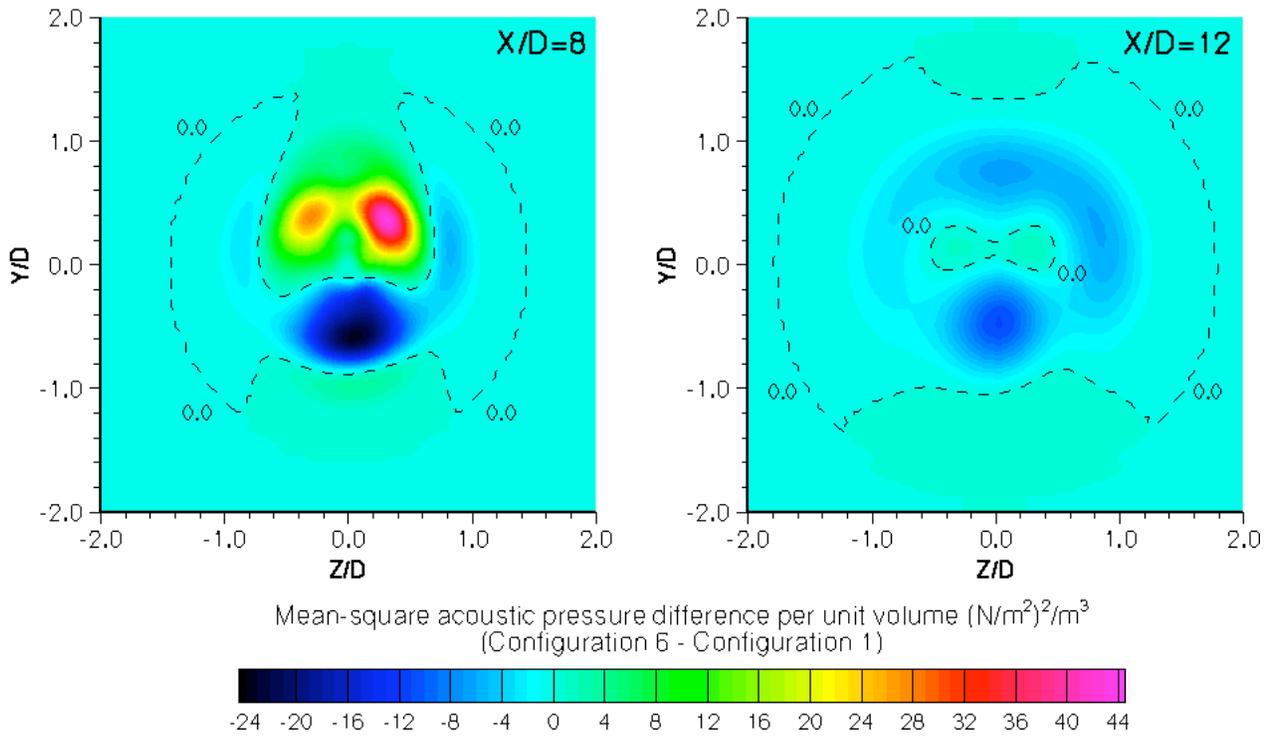
**Figure 24: Noise source difference map (configuration 6 – configuration) 1 at X/D=8 and 12**
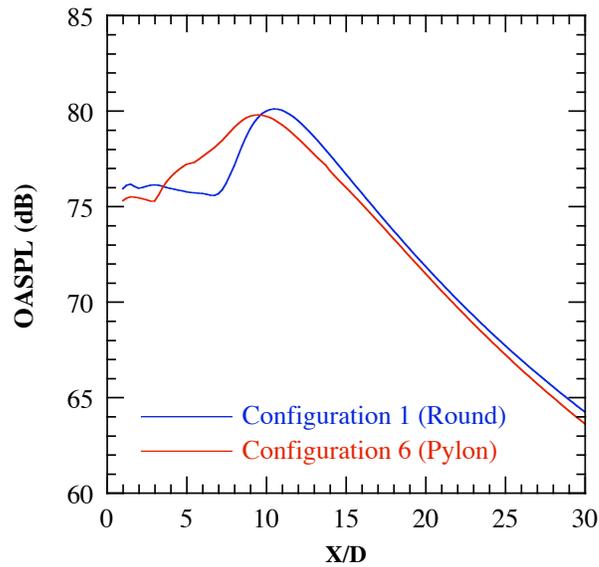

Figure 25: OASPL histogram for configurations 1 and 6
(Note: OASPL levels for configuration 6 have been adjusted to account for pylon area)